Combining a Large Aperture Scintillometer and estimates of available energy to derive evapotranspiration over several agricultural fields in sermi-arid regions.

J. Ezzahar, A. Chehbouni, J.C.B. Hoedjes, S. Er-Raki

HAL Id: ird-00389765
http://hal.ird.fr/ird-00389765

Submitted on 29 May 2009

Manuscript Information	
Journal Acronym	**TPLB**
Volume and issue	
Author name	
Manuscript No. (if applicable)	**_A_371173**

QUERIES: to be answered by AUTHOR

Dear Author
Please address all the numbered queries on this page which are clearly identified on the proof for your convenience.
Thank you for your cooperation

QUERY NO.	QUERY DETAILS
1	**Is this Equation 9?**
2	**Allen et al. not in refs list, please give details.**
3	**Please cross-reference the text without the use of section numbers!**
4	**Please update reference if possible.**

Taylor & Francis
Taylor & Francis Group

Combining a large aperture scintillometer and estimates of available energy to derive evapotranspiration over several agricultural fields in a semi-arid region

JAMAL EZZAHAR[1], ABDELGHANI CHEHBOUNI[2], SALAH ER-RAKI[1] & LAHOUCINE HANICH[3]

[1]*Center for Research on Water in Arid and Semi-arid Environments, Faculty of Sciences and Technology, University Caddi Ayyad, Marrakech, Morocco,* [2]*Centre d'Etudes Spatiales de la Biosphère BP 31401 cedex Toulouse, France, and* [3]*Hydrogeology Department, Faculty of Sciences and Technology, University Caddi Ayyad, Marrakech, Morocco*

Abstract

The objective of the present study was to investigate the potential of a large aperture scintillometer (LAS) combined with a simple available energy model to estimate area-averaged latent heat flux in difficult environmental conditions. The difficulties are related to the sparseness of the vegetation, the heterogeneity of the soil characteristics, and, most importantly, the heterogeneity in terms of soil moisture induced by the "flood irrigation" method. In this context, three sites (Agdal, R3 and Sâada) in the Tensift Al Haouz plain (region of Marrakech city, central Morocco) have been equipped with a LAS and eddy covariance (EC) system (local scale measurements). Agdal and R3 are a flood-irrigated olive yard and wheat field, respectively. Sâada is a drip-irrigated orange orchard. Due to the irrigation method applied, the Agdal and R3 sites shifted from being almost homogeneous between two irrigations (dry conditions) and completely heterogeneous during the irrigation events (large variability of soil moisture along the site), while Sâada was always heterogeneous, at least at the scintillometer footprint scale. Consequently, the comparison between the sensible heat fluxes derived from both LAS and EC showed a large scatter during the irrigation events, while a good correspondence was found in between two irrigations. It was also found that combining LAS and an estimate of the available energy (using a simple model) can provide reasonable large-scale evapotranspiration estimates, which are of prime interest for irrigation management.

Keywords: *Evapotranspiration, olive, orange, scintillation, semi-arid region, whea*

Introduction

In southern Mediterranean regions, as well as other arid and semi-arid regions of the world, water availability is extremely limited due to poor and irregular rainfall, high evaporation, and inadequate water management (Centritto et al. 2000). Irrigated agriculture represents the major water user (about 80–90% of total available water), with an efficiency which does not exceed 50% (Chehbouni et al. 2008b). Therefore, sound and efficient irrigation management is an important step for achieving sustainable management of water resources in these regions (Centritto et al. 2005; Tahi et al. 2007). In this regard, estimates of evapotranspiration (ET) are strongly needed over large and heterogeneous surfaces (at the irrigation district scale). However, obtaining ET at this scale is not a trivial task. Indeed, the surface heterogeneity caused either by the contrast in soil moisture or vegetation type and cover generates a large spatial variability of fluxes which limit the use of local scale measurement devices such as the eddy covariance (EC) system, unless one deploys a network of EC devices, which is not always technically and economically feasible.

Optical satellite remote sensing can be considered as a promising data source for deriving regional ET at the time of satellite overpass. However, their benefit for water management is limited, since solely the instantaneous values of ET can be obtained from satellite data, while the main interest of water managers is the daily value of ET (Bastiaanssen

et al. 2000). Such instantaneous estimates can be combined with aggregation methods so that diurnal values of regional ET can be derived (Chehbouni et al. 2008c). Nevertheless, the effectiveness of this approach cannot be fully assessed without a validation of the modeled fluxes using areally averaged surface flux measurements under different conditions which is, for the reasons mentioned above, not always feasible on an operational basis.

In this context, scintillometry can be considered as an attractive method for routinely measuring area-averaged convective fluxes. Indeed, several studies have demonstrated its potential to estimate the diurnal course of the surface fluxes over natural (and thus heterogeneous) landscapes (Chehbouni et al. 1999, 2000, 2008b; Lagouarde et al. 2002; Meijninger et al. 2002a; Asanuma et al. 2006; Ezzahar et al. 2007a). Consequently, the large aperture scintillometer (LAS) has recently become very popular especially since, in contrast to EC systems, it requires little maintenance, and its cost is very reasonable. The LAS provides integrated sensible heat flux directly over several kilometers; the latent heat flux can be obtained indirectly as the residual term of the energy balance equation providing estimates of available energy which can be easily derived from remote sensing (Meijninger et al. 2002b; Ezzahar et al. 2007b).

The present study reports the results of an evaluation exercise aimed at combining LAS with an estimate of available energy to derive ET over the dominant crop types (olive, orange and wheat) in the Tensift Al Haouz plain (region of Marrakech city, central Morocco). The final purpose is to improve water management at the irrigation district scale. The challenge is then deriving the flux over orchards that are characterized by tall vegetation and strong soil moisture contrasts due to irrigation practices. The data were collected within the framework of the SUDMED (Chehbouni et al. 2008a) and IRRIMED (http://www.irrimed.org) programmes.

Theoretical background

Estimation of sensible heat flux, H_{LAS}, with LAS

In this section, we briefly recall the principles of the determination of turbulent sensible heat flux with LAS. For a complete description, the reader can refer to Clifford et al. (1974), Hill et al. (1992) and Hill (1997).

The LAS provides a measurement of the structure parameter for the refractive index (C_n^2) along the optical path. This C_n^2 can be related to the structure parameter C_T^2 for temperature by (Wesely 1976):

$$C_T^2 = C_n^2 \left(\frac{T^2}{\gamma p}\right)^2 \left(1 + \frac{0.03}{\beta}\right)^{-2}, \quad (1)$$

where γ is the refractive index coefficient for air (7.8×10^{-7} KPa^{-1}), p is the atmospheric pressure (Pa), T the air temperature (K) and β the Bowen ratio. The final bracketed term is a correction for the effects of humidity. C_n^2 and C_T^2 are in (m$^{-2/3}$) and (K^2 m$^{-2/3}$), respectively.

Once C_T^2 is known, the sensible heat flux can be derived from the Monin–Obukhov Similarity Theory (MOST), which depends on the stability parameter ζ ($= (z_{LAS} - d)/L_{OB}$, where z_{LAS} and d are the effective height of the LAS above the surface and the displacement height, respectively. L_{OB} is the Monin–Obukhov length (m) given by:

$$L_{OB} = \frac{Tu_*^2}{\kappa g T_*}, \quad (2)$$

with κ the von Karman constant (0.41), g the gravity (9.81 ms^{-2}), $T_*(= -\overline{w'T'}/u_*$, w' and T' vertical wind speed and temperature fluctuations, respectively) the temperature scale and $u_\star$ the friction velocity (ms^{-1}):

$$u_* = \kappa u [\ln((z_{LAS} - d)/z_0) - \psi(\zeta)]^{-1}, \quad (3)$$

u is the wind speed and ψ is the integrated stability function defined for unstable conditions ($\zeta < 0$) as (Panofsky & Dutton 1984)

$$\psi(\zeta) = 2\ln\left[\frac{1+x}{2}\right] + \ln\left[\frac{1+x^2}{2}\right] - 2\arctan(x) + \frac{\pi}{2}, \quad (4)$$

$$\text{with } x = (1 - 16\zeta)^{1/4}. \quad (5)$$

According to MOST, it is possible to link C_T^2 and $T_\star$ for unstable conditions, i.e. $\zeta < 0$:

$$\frac{C_T^2(z_{LAS} - d)^{2/3}}{T_*^2} = f(\zeta) = c_1(1 - c_2\zeta)^{-2/3}, \quad (6)$$

where c_1 and c_2 are empirical constants given by De Bruin et al. (1993) as 4.9 and 9, respectively.

The sensible heat flux H_{LAS} can be then computed iteratively as:

$$H_{LAS} = -\rho c_p T_* u_*, \quad (7)$$

where ρ and c_p are the density and specific heat capacity of the air, respectively.

During the iteration, β is calculated using H_{LAS}, net radiation (R_n) and soil heat flux (G):

$$\beta = \frac{H_{LAS}}{R_n - G - H_{LAS}}. \quad (8)$$

In this study, d and z_0 were calculated according to the classical rule-of-thumb as follows:

$$d \approx 2h/3 \text{ and } z_0 = 0.13h,$$
$$\text{with } h \text{ the vegetation height.} \quad (9)$$

Estimation of available energy

Net radiation. Net radiation (R_n), which represents the balance of short- and long-wave radiation reaching and leaving the surface, can be expressed as:

$$R_n = (1 - \alpha)R_g + \varepsilon_S R_a - R_t, \quad (10)$$

where α is surface albedo, R_g is global solar radiation (Wm^{-2}), ε_s is surface emissivity which has a almost constant value (in practical work a value of 0.98 may be taken for crop canopies (Ortega et al. 2000)), R_a is atmospheric radiation (Wm^{-2}), and R_t is the terrestrial radiation emitted by the surface (Wm^{-2}). The radiative balance in the solar domain, $(1 - \alpha)R_g$, is the principal component of Equation 10 during the daytime. The radiation balance in the thermal domain, $\varepsilon_s R_a - R_t$, usually has a lower value but it is the only component of the net radiation at night. Using the Stefan–Boltzman equation (Monteith & Unsworth 1990), R_a and R_t can be expressed as a function of air and surface temperatures, respectively. Then, Equation 10 can be rewritten as:

$$R_n = (1 - \alpha)R_g + \varepsilon_S \sigma(\varepsilon_a T_a^4 - T_{surf}^4), \quad (11)$$

where ε_a is the atmospheric emissivity, T_a is the air temperature (K), T_{surf} is the surface temperature (K), and σ is the Stefan–Boltzman constant ($5.67 \times 10^{-8}\ \text{Wm}^{-2}\text{K}^{-4}$).

Many authors have proposed empirical relationships which relate the atmospheric emissivity to the air temperature (Angstrom 1918; Brunt 1932; Idso et al. 1981). In the current study, we used the expression proposed by Brutsaert (1975) where ε_a is computed from air temperature and vapour pressure as:

$$\varepsilon_a = 1.24(e_a/T_a)^{1/7},$$

with e_a the air vapour pressure (hPa).

Soil heat flux. The soil heat flux is an important component of the surface energy balance. Due to the complexities of surface cover and physical processes occurring in the soil, the soil heat flux is the most difficult scalar to measure accurately at the appropriate space-scale. In the literature, G at the surface is often estimated as a fraction of net radiation (Brutsaert 1982; Stull 1988; Humes et al. 1994; Kustas & Goodrich 1994; Villalobos et al. 2000).

In this study, we used the simple formula proposed by Su et al. (2001) as follows:

$$G = R_n[\Gamma_c + (1 - f_c)(\Gamma_s - \Gamma_c)]\ (\text{Wm}^{-2}), \quad (12)$$

in which they assume the ratio of soil heat flux to net radiation $\Gamma_c = 0.05$ for full vegetation canopy (Monteith 1973) and $\Gamma_s = 0.315$ for bare soil (Kustas & Daughtry 1989).

Provided that sensible heat flux is measured by the LAS, net radiation and soil heat flux are obtained using the above formulas, and latent heat flux, $L_v E_{LAS}$, can be derived as the residual term of the energy balance equation as follows:

$$L_v E_{LAS} = R_n - G - H_{LAS} \quad (13)$$

Experiment

Site description

The region of interest is the Tensift Al Haouz plain (region of Marrakech city, central Morocco), characterized by a semi-arid Mediterranean climate, i.e. the atmosphere is very dry, with an average relative humidity of 56%. The evaporative demand is very high [around 1600 mm/yr according to reference evapotranspiration estimates (Allen et al. 1998)], greatly exceeding the annual rainfall ranging from 192 to 253 mm year^{-1}. Most of the precipitation falls during winter and spring, from the beginning of November until the end of April. Major irrigated vegetation types in the region include wheat, olive and orange. The irrigation uses either ground water or the water stored in the dams. In this study, three sites named "Agdal", "R3" and "Sâada", have been equipped with micrometeorological instruments.

Agdal site. The Agdal site is a flood-irrigated olive yard, which is located in the southeast of the city of Marrakech, Morocco (31°36′N, 07°59′W). Figure 1a displays the area of interest on a very high spatial resolution image acquired by the Quickbird satellite (0.62 and 2.4 m in panchromatic and multi-spectral, respectively). The experiment was set up in the southern part of the Agdal site on an area, of about 700 × 800 m, surrounded by orange and olive trees (Figure 1a). The average height of the olive trees is 6 m with a mean fraction cover of about 55%, as obtained from hemispherical canopy photographs (using a Nikon Coolpix 950® with a FC-E8 fish-eye lens converter, field of view 183°).

Two water basins are used for irrigation. Water is manually diverted to every tree through a ditch network. Each tree is surrounded by a small earthen levy which retains irrigation water, and ensures water supply for every tree (Williams et al. 2004). Irrigation

starts from the southern border of the field, and, depending on available manpower, progresses towards the northern border of the site over approximately 12 days. More details about the site and experimental set-up are presented in Ezzahar et al. (2007a) and Hoedjes et al. (2007).

R3 site. The R3 site is located approximately 45 km east of Marrakech (31°68′N, 7°38′W) (Figure 1b). It is an irrigated area, managed by the ''ORMVAH'' (Office Régional de Mise en Valeur Agricole du Haouz) since 1999. The main crop grown in R3 is wheat, which is generally sown between mid-November and mid-January, depending on climatic conditions and the start of the rainfall season. The ORMVAH manages the distribution of water starting from December through May. The frequency and the amount of water for each irrigation are predetermined according to the dam water level at the beginning of the cropping season without any consideration for the actual surface soil moisture status and atmospheric demand. Additionally, flood irrigation is the most widely used method in this district. More details about the site are presented in Duchemin et al. (2006) and Er-Raki et al. (2007).

Sâada site. Sâada is a drip-irrigated orange orchard, which is located approximately 15 km west of Marrakech (31°37′36″N, 08°09′35″W) (Figure 1c). The density of the orange trees is about 70%, as calculated from hemispherical canopy photographs (using a Nikon Coolpix 950® with a FC-E8 fish-eye lens converter, field of view 183°). The average height of the trees was about 3 m. The site was maintained in well-watered conditions by daily irrigation using pipelines placed close to each tree. The site is divided into several sectors. More than one sector situated in different places was irrigated at the same time; those sectors are shown with the same colour in Figure 2. With this irrigation network, the site can be considered as heterogeneous, at least at the scintillometer footprint scale.

Flux and micrometeorological measurements

The three sites were equipped with a set of standard meteorological instruments to measure wind speed and direction, air temperature and humidity. Additionally, net radiation, soil heat flux, radiative soil and vegetation temperatures and soil moisture were also measured. The different micro-meteorological instruments used in this study and their locations are summarized in Table I. Measurements were sampled at 1 Hz, averaged, and then stored at 30-min intervals on a CR10X datalogger. Each site was also
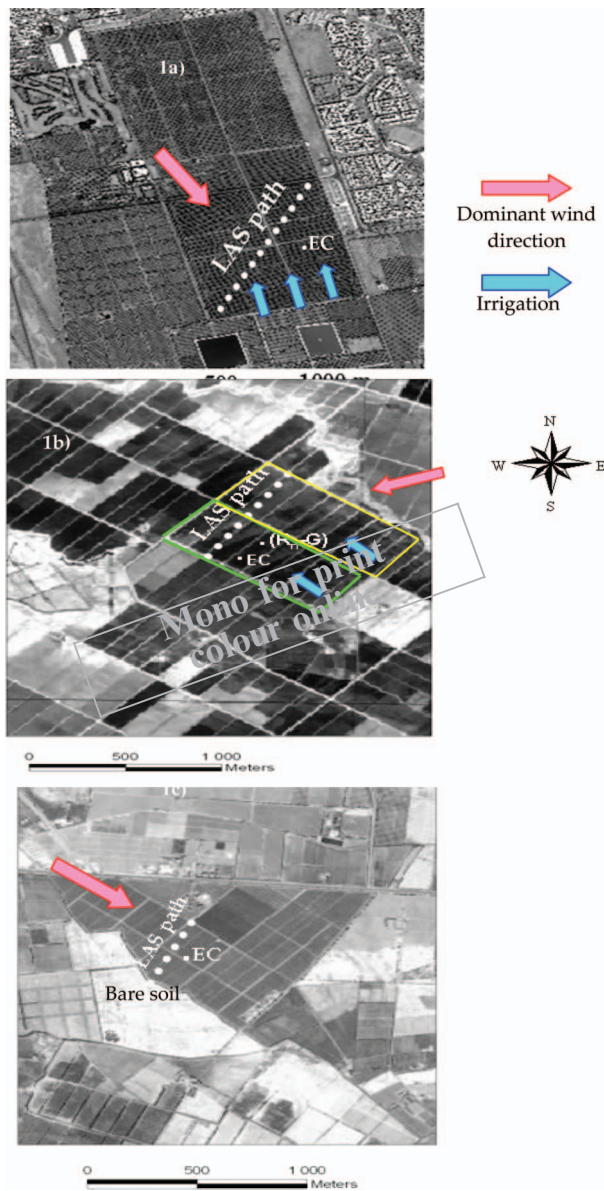

Figure 1. Overview of the three sites (Quickbird images). The LAS path and the location of the EC system are shown (1a for Agdal, 1b for R3 and 1c for Sâada). The main wind direction and the irrigation are also shown.
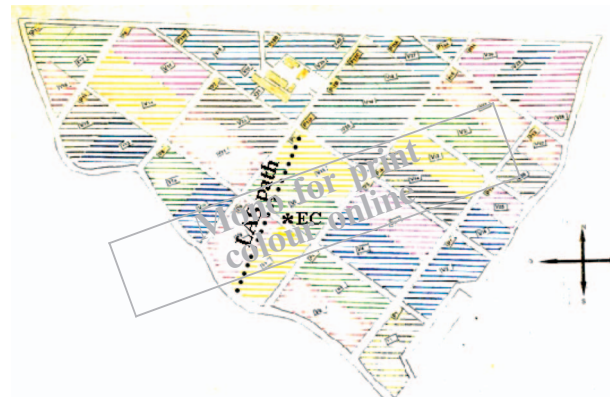

Figure 2. Overview of the irrigation method at the Sâada site. The sectors having the same colour are irrigated at the same time.

Table I. Overview of the different micrometeorological instruments used over the three sites.

Site	Agdal	R3	Sâada
Time	Between DOY 212 and 243 (2003)	Between DOY 73 and 143 (2003)	Between DOY 139 and 174 (2004)
Air temperature and relative humidity	Vaisala HMP45AC (9 m)	Vaisala HMP45AC (2 m)	Vaisala HMP45AC (4 m)
Wind speed and direction	Young Wp200 (9 m)	Young Wp200 (3 m)	Young Wp200 (4 m)
Net radiation	CNR1 radiometer (Kipp & Zonen) (9 m)	Q7 net radiometer (REBS) (2 m)	CNR1 radiometer (Kipp & Zonen) (4.3 m)
Soil heat flux	Heat flux plates (HFT3-L) (1 cm)	Heat flux plates (HFT3-L) (5 cm)	Heat flux plates (HFT3-L) (1 cm)
Radiative soil and vegetation temperatures	Precision Infrared temperature sensor (IRTS-P) (1 and 7.15 m)	Precision Infrared temperature sensor (IRTS-P) (2 m)	Precision Infrared temperature sensor (IRTS-P) (1 and 3.5 m)
Soil moisture	CS616 water content reflectometer (5 cm)	Theta probe	CS616 water content reflectometer (5 cm)
Sensible heat flux	3D sonic anemometer (Eddy covariance method 9.2 m)	3D sonic anemometer (Eddy covariance method 2 m)	3D sonic anemometer (Eddy covariance method 6.9 m)
	Large Aperture Scintillometer (14 m)	Large Aperture Scintillometer (4.5 m)	Large Aperture Scintillometer (9.2 m)
Latent heat flux	Krypton hygrometer (KH20) (Eddy covariance method 9.2 m)	Krypton hygrometer (KH20) (Eddy covariance method 2 m)	Open-path infra-red gas analyser (LICOR-7500) (Eddy covariance method 6.9 m)
	Large Aperture Scintillometer (energy balance equation) (14 m)	Large Aperture Scintillometer (energy balance equation) (4.5 m)	Large Aperture Scintillometer (energy balance equation) (9.2 m)

equipped with an EC system which provides high-frequency measurements of the three dimensional (3D) air velocity and temperature fluctuations (see Table I). For site R3, the 10 Hz data were processed directly online, and the half-hourly fluxes were stored on a CR23X datalogger (Campbell Scientific Inc., USA).

At the Agdal and Sâada sites, the raw measurements recorded on a CR5000 datalogger were processed to calculate sensible heat fluxes (using the average of the covariance between vertical wind speed and temperature fluctuations) and latent heat fluxes (using the average of the covariance between vertical wind speed and humidity fluctuations). This calculation was performed at half-hour intervals using the post processing "Ecpack" software package. This software was developed by the Meteorology and Air Quality Group at Wageningen Agricultural University (The Netherlands), and it is available for download at http://www.met.wau.nl/. During processing, all required corrections are performed: planar fit correction (Wilczak et al. 2001), correcting the sonic temperature for the presence of humidity (Schotanus et al. 1983), frequency response corrections for slow apparatus and path length integration (Moore 1986; Horst 1999), the inclusion of the mean vertical velocity according to Webb et al. (1980), and O_2 correction for the O_2-sensitive Krypton hygrometer (Van Dijk et al. 2003).

LAS measurements were made over the three sites. The LAS used here was built by the Meteorology and Air Quality Group at Wageningen. It has an aperture size of 0.15 m, and the wavelength of the light beam emitted by the transmitter is 940 μm. At the receiver, C_n^2 was sampled at 1 Hz and averaged over 1-min time steps by a CR510 datalogger (Campbell Scientific Ltd.). The path lengths were about 1050, 690 and 500 m for Agdal, R3 and Sâada sites, respectively (see Figures 1a, 1b and 1c). Figure 3 presents the daytime wind direction during the experiment for the three sites. The frequency analysis of wind direction showed that the dominating directions were north-west, north-east to east, and north-west for Agdal, R3 and Sâada, respectively.

Results and discussion

Energy balance closure

One approach for testing data quality is to test for closure of the surface energy balance (Wilson et al. 2002). By ignoring the term of canopy heat storage (Scott et al. 2003; Testi et al. 2004) and assuming the principle of conservation of energy, the energy balance closure is defined as $R_n - H_{EC} - L_v E_{EC} - G$ and should be close to zero (H_{EC} and $L_v E_{EC}$ are the sensible and latent heat fluxes derived from the EC
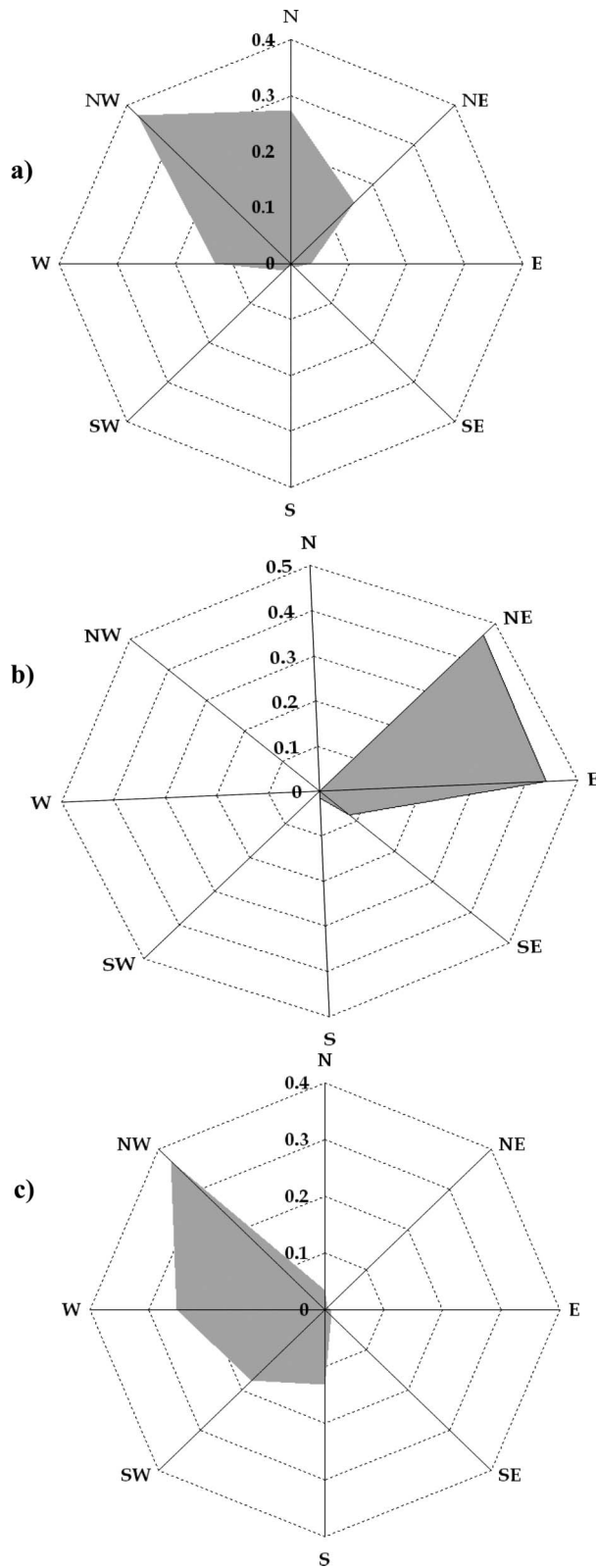
Figure 3. The daytime wind direction over the three sites Agdal (a), R3 (b), and Sâada (c).

representative of the flux source area. Most results in the literature have shown that independent measurements of the energy balance flux components were generally not consistent with the principle of energy conservation. The sum of latent and sensible heat fluxes measured by the EC system was often less than the available energy (Twine et al. 2000; Hoedjes et al. 2002; Testi et al. 2004; Chehbouni et al. 2008b).

Figure 4 shows the plot of $AE_{mes} = R_n - G$ against $H_{EC} + L_v E_{EC}$ for the Agdal, R3 and Sâada sites under daytime conditions. Table II presents the statistics of the results associated with each site. In this table the linear regression, coefficient correlation and the Root Mean Square Error (RMSE), defined as the square root of the averaged quadratic difference between observations and simulations, are presented. Over all fields, the available energy was systematically higher than the sum of sensible and latent heat fluxes. The absolute value of average closure was about 20% of available energy over R3, 8% over Sâada and 8% over Agdal. It can be seen that the difference in the R3 site is larger than in Sâada and Agdal. Several reasons can be suggested to explain this difference.

(a) A part of this difference can be related to the use of the measured soil heat flux at 5 cm in the R3 site, while in the two other sites, the measurement depth of G was 1 cm.

(b) The measurements of $(R_n - G)$ were made far from the EC system (Figure 1b); consequently the impact, in terms of the source area, influences considerably the energy balance closure. For the Sâada and Agdal sites, $(R_n - G)$ was measured close to the EC system.

(c) At the Agdal and Sâada sites, net radiation was measured using the CNR1 radiometer (Kipp and Zonen) which is more reliable than the radiometer Q7 (REBS) used at R3, and this may also have generated some error (Kustas et al. 1998).

(d) The EC fluxes in R3 were processed directly online on the CR23X datalogger. Only the mean vertical velocity is included according to Webb et al (1990). The effect of frequency response on sensors, sensor separation, path-length averaging and signal processing time (Moore 1986) were not considered. Testi et al. (2004) have shown that the sum of these corrections indicate typically 11% of flux loss. This could account for the obtained underestimates of the EC fluxes.

However, compared to what has been reported in other experimental studies [the average error in closure ranges from 10 to 30% according to Twine et al. (2000)], the energy balance closure obtained
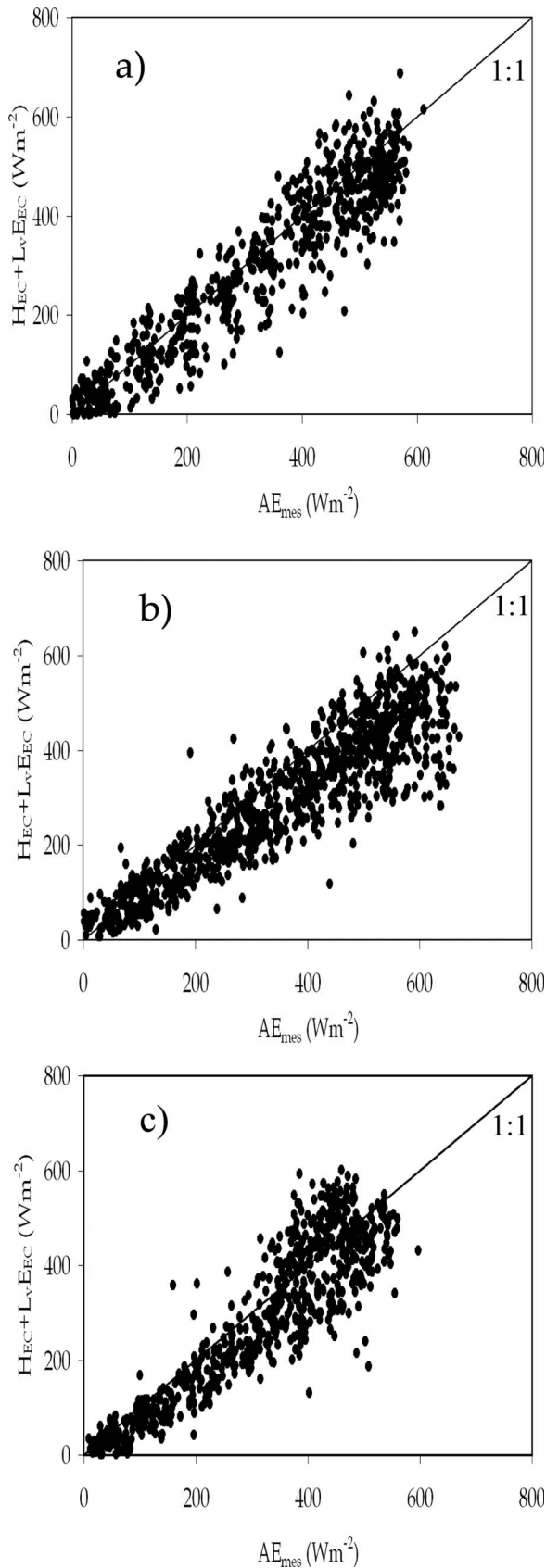
system). The energy balance closure depends both on the EC measurements and on the ability to adequately quantify the available energy over an area

Figure 4. Comparison between measured available energy ($AE = R_n - G$) and the sum of eddy covariance measurements ($H_{EC} + L_vE_{EC}$) over the three sites (4a for Agdal, 4b for R3 and 4c for Sâada).

here can be considered acceptable especially if one bears in mind the complexities of the study sites.

Comparison of sensible heat fluxes

During this study, Agdal and R3 sites shifted from being almost homogeneous between two irrigations (dry conditions) to completely heterogeneous during the irrigation events (large variability of soil moisture along the site), while Sâada was always heterogeneous, at least at the scintillometer footprint scale.

A comparison between LAS-based estimates of sensible heat flux and those measured by the EC method, in both homogeneous and heterogeneous conditions, is made. We will solely consider the unstable conditions (i.e. $L_{OB} < 0$), since the behaviour of the temperature structure parameter is not well known for stable conditions especially for tall and sparse vegetation. The sensible heat fluxes from LAS are obtained by iteration using Equations 1–7, with the values of T, u, R_n, and G measured close to the location of the EC system.

Homogeneous conditions (before an irrigation event). In general the "source area" (the area for which the surface flux measurements is representative) of the EC is very small compared to that of LAS. This has been investigated in more detail by Ezzahar et al. (2007b) and Hoedjes et al. (2007). An example of the dimensions of the source area of the EC and LAS, calculated using the Footprint model (Horst & Weil 1994), is presented in Figure 5. The theoretical background of the calculation of the source area is described in detail in Ezzahar et al. (2007b) and Hoedjes et al. (2007).

In Figures 6a and 6b, the sensible heat fluxes obtained from LAS (H_{LAS}) are compared, under homogeneous conditions (before an irrigation event), with those measured by the EC (H_{EC}) for the Agdal and R3 sites, respectively. The statistical results are shown in Table II. In spite of the difference in the size of the source areas of the LAS and EC system, results showed that the sensible heat flux derived from LAS agreed fairly well with those measured by the EC system for both sites. Therefore, it can be concluded that the sites are relatively homogeneous before an irrigation event. In addition, the obtained results can be considered very encouraging for the Agdal site, because the transfer processes in such a field as Agdal, which is covered with tall and sparse vegetation, are more complicated than over short crops.

Heterogeneous conditions (irrigation event). The irrigation is applied from the southern border of the site and progresses slowly towards the northern border at the Agdal and R3 sites. This causes the two source

Table II. Statistical results of the comparison between
(a) measured available energy ($AE = R_n - G$) and the sum of EC measurements ($H_{EC} + L_vE_{EC}$) over the three sites.
(b) LAS and EC sensible heat fluxes, H_{LAS} and H_{EC}, respectively, during homogeneous conditions (before an irrigation event) and during heterogeneous conditions (irrigation event).
(c) Estimated (AE_{est}) and measured (AE_{mes}) available energy over the three sites.
(d) Measured (derived from the EC system L_vE_{EC}) and simulated (derived from LAS using the estimated available energy, L_vE_{LAS}) evapotranspiration.

| Site	R3	Agdal	Sâada
Sensible heat flux Homogenous conditions	$H_{LAS} = 0.86H_{EC} + 14.63$ $R^2 = 0.93$ RMSE $= 41.8$ Wm^{-2}	$H_{LAS} = 0.81H_{EC} + 25$ $R^2 = 0.93$ RMSE $= 33.6$ Wm^{-2}	
Sensible heat flux Heterogeneous conditions	$H_{LAS} = 0.81H_{EC} + 28$ $R^2 = 0.8$ RMSE $= 41.27$ Wm^{-2}	$H_{LAS} = 0.60H_{EC} + 65.26$ $R^2 = 0.55$ RMSE $= 55.61$ Wm^{-2}	$H_{LAS} = 0.68H_{EC} + 79.67$ $R^2 = 0.61$ RMSE $= 63.28$ Wm^{-2}
Energy balance closure	$H_{EC} + L_vE_{EC} = 0.77AE_{mes} + 18.89$ $R^2 = 0.84$ RMSE $= 98$ Wm^{-2}	$H_{EC} + L_vE_{EC} = 0.92AE_{mes} + 0.05$ $R^2 = 0.88$ RMSE $= 66$ Wm^{-2}	$H_{EC} + L_vE_{EC} = 0.98AE_{mes} - 20.3$ $R^2 = 0.82$ RMSE $= 74$ Wm^{-2}
Avaible energy (AE)	$AE_{est} = 0.9AE_{mes} - 17.39$ $R^2 = 0.92$ RMSE $= 74$ Wm^{-2}	$AE_{est} = 0.94AE_{mes} + 14.24$ $R^2 = 0.98$ RMSE $= 23$ Wm^{-2}	$AE_{est} = 1.01AE_{mes} + 7$ $R^2 = 0.96$ RMSE $= 42$ Wm^{-2}
Latent heat flux	$L_vE_{LAS} = 1.11L_vE_{EC} - 3.56$ $R^2 = 0.74$ RMSE $= 49$ Wm^{-2}	$L_vE_{LAS} = 0.91L_vE_{EC} + 25.6$ $R^2 = 0.71$ RMSE $= 56$ Wm^{-2}	$L_vE_{LAS} = 1.34L_vE_{EC} - 60.38$ $R^2 = 0.68$ RMSE $= 62$ Wm^{-2}
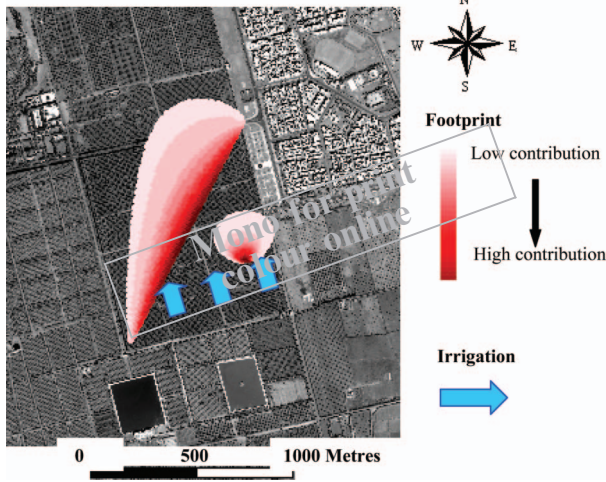
Figure 5. Source areas of the LAS and EC system are shown in red (calculated using the footprint model of Horst & Weil 1994) and the irrigation schedule in blue.

areas of LAS and of the EC system to be no longer comparable in terms of soil moisture and, thus sensible heat flux. Figures 7a and 7b show the plot of H_{LAS} against H_{EC} for the Agdal and R3 sites, respectively. The statistical results are presented in Table II. For Agdal, the irrigation is applied in such a manner that, due to prevailing wind directions, the small source area of the EC will be irrigated much sooner than the large area of the LAS, which explains

the overestimation of the H_{LAS}. As irrigation proceeds, the EC source area starts to dry out before the entire source area of LAS is irrigated, consequently the H_{EC} overestimates the H_{LAS}. For site R3, the irrigation is applied in a direction more or less parallel to the main wind direction and the green sector will be irrigated after the entire yellow sector is irrigated (see Figure 1b). Therefore, the source area of LAS will be a mixture of dry and wet surfaces, while the small source area of the EC will be wet when the irrigation arrives around the tower. Consequently, during the irrigation, a difference in the surface characteristics of the source areas of the two methods will occur.

In addition, it can be noticed that the effect of irrigation is clearer in the Agdal site than in the wheat site. This is because, in the latter, 35 mm of rainfall had fallen just before the irrigation event, and the ORMVAH cannot stop the irrigation in order to keep the order for the next irrigation event. For Sâada, the irrigation method is different from that applied in Agdal and R3 sites. As shown in Figure 2, irrigation is applied in such manner that several sectors, located in different places, were irrigated at the same time; this can also generate large differences in the soil moisture between the source areas of the LAS and EC system. In Figure 7c, H_{LAS} is compared to H_{EC}. The statistical results are presented in Table II. In addition to the predicted discrepancy between the LAS-based sensible heat fluxes and
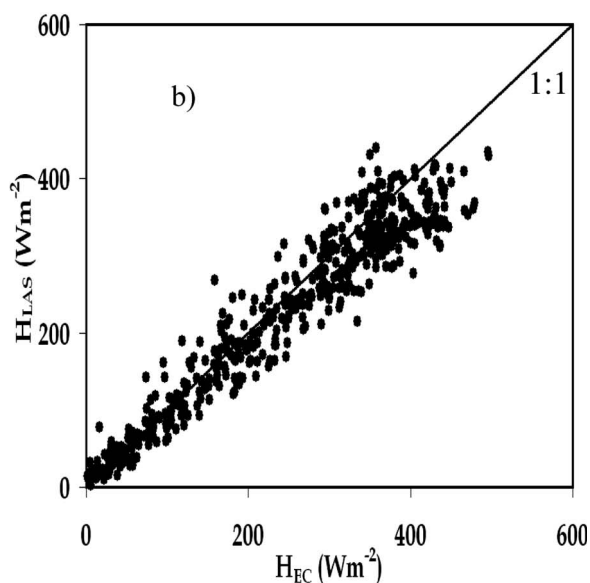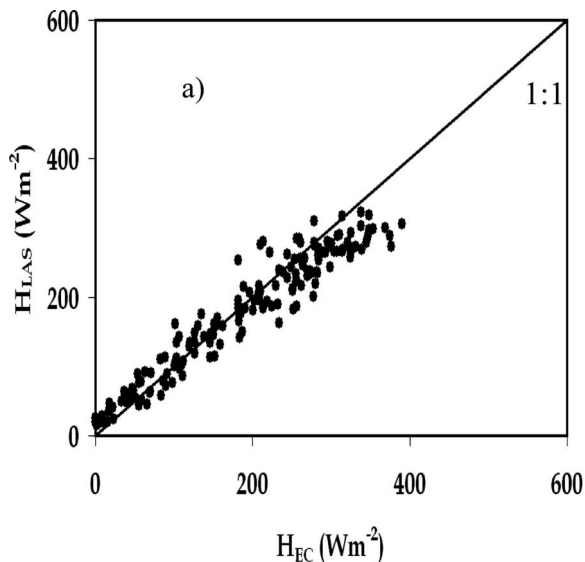
Figure 6. Comparison of H_{LAS} and H_{EC} during homogeneous conditions (before an irrigation event) for Agdal (a) and R3 (b) sites.

those measured by the EC system due to the irrigation method, the comparison showed a large overestimation of the H_{LAS} for low values (within the circle shown in Figure 7c). This is in large part caused by the advection of dry, warm air from the area surrounding the field (bare soil).

Comparison of latent heat fluxes

Since we are interested in the determination of the latent heat flux from LAS (L_vE_{LAS}) in an operational context, a simple model for the estimation of the available energy, $AE_{est}(=(R_n - G)_{est})$, is proposed in this study (see § 2.2). Thus L_vE_{LAS} is estimated as the residual term of the energy balance equation: $L_vE_{LAS} = AE_{est} - H_{LAS}$. In order to quantify the
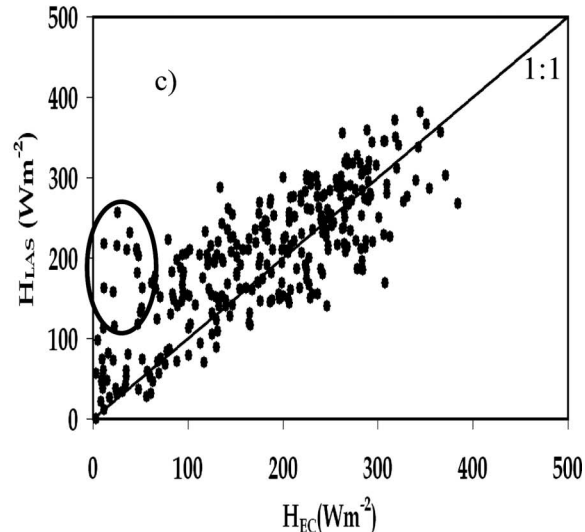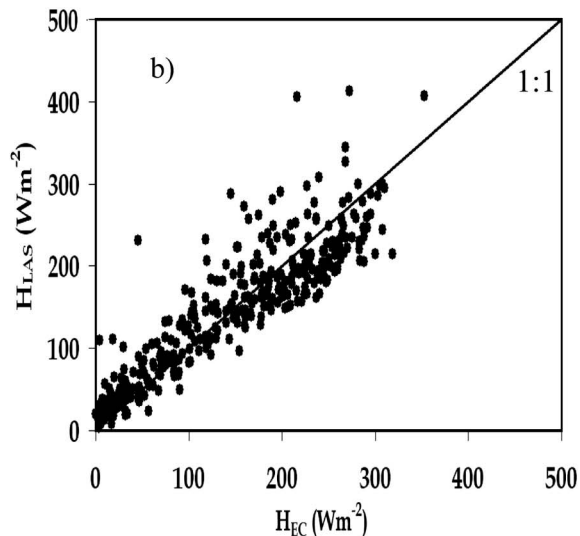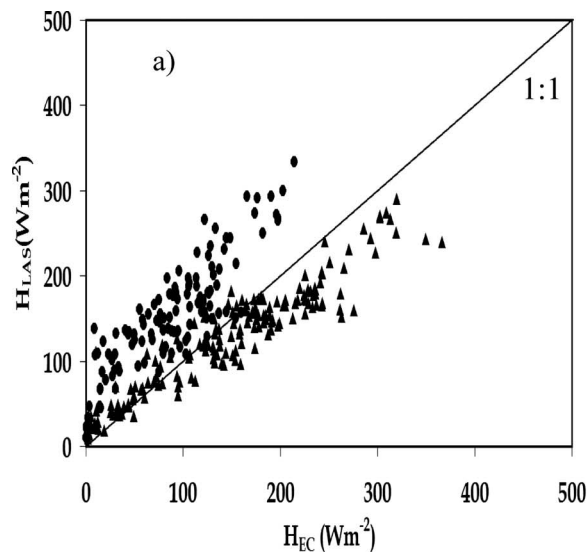

Figure 7. Comparison of H_{LAS} and H_{EC} during heterogeneous conditions (the irrigation event) for Agdal (a), R3 (b) and Sâada (c) sites. At Agdal the circles represent the days when the LAS source area was dry and the EC source area was wet (irrigated); the triangles represent the days when the EC source area started to dry out and the LAS source area was wet (irrigated).

error associated to the estimated available energy in the estimation of the LvE$_{LAS}$, a comparison between AEest and AEmes was made over the three sites. AEest was estimated using the following considerations.

(a) The albedo and the global radiation were calculated from the CNR1 which measures the incoming and outgoing solar and far-infrared radiation. For site R3, we used the data taken from the CNR1 installed over another wheat field. The fields were close by and very similar.

(b) The surface emissivity is assumed to be 0.98 (Ortega-farias et al. 2002).

(c) The vegetation cover was calculated from hemispherical canopy photographs. Further details about this technique are given in Er-Raki et al. (2007).

(d) The surface temperature, T_{Surf}, was calculated from the Precision Infrared Temperature Sensor (IRTS-P). For Agdal and Sâada sites, T_{Surf} was estimated from measured soil (T_s) and canopy (T_c) temperatures weighted by the fractional area of vegetation (Norman et al. 1995):

$$T_{surf} \approx \left[f_c T_c^4 + (1 - f_c) T_s^4 \right]^{1/4},$$
where f_c is the vegetation cover.

Figures 8a, 8b, and 8c present comparisons between AEest and AEmes for Agdal, R3 and Sâada, respectively. The statistical results are presented in Table II. The RMSE were 23, 74 and 42 W m^{-2} for Agdal, R3 and Sâada, respectively. By analysing these results, it emerges that the comparison yields more discrepancies at R3 than Agdal and Sâada. This scatter was expected due to the climatic conditions of the R3 site, which influence the calculation of atmospheric emissivity. The latter was derived using Brutsaert's formula, which was established for clear-sky conditions only. The R3 experiment was carried out during the rainy season, therefore several cloudy days occurred, while most of the days during the Agdal and Sâada experiments were sunny. This was very evident when we compared the solar radiation over the three sites (not shown). Despite this scatter, it can be concluded that the simple model used to estimate the available energy works fairly well over the three sites, at least at the local scale.

Finally, the L$_v$E$_{LAS}$ obtained as the residual term of the energy balance equation, using the *AE*est and H$_{LAS}$, is compared with the L_vE_{EC} in Figures 9a, 9b and 9c for Agdal, R3 and Sâada, respectively. These comparisons include the homogeneous and heterogeneous conditions. The statistical results are presented in Table II. This discrepancy can be
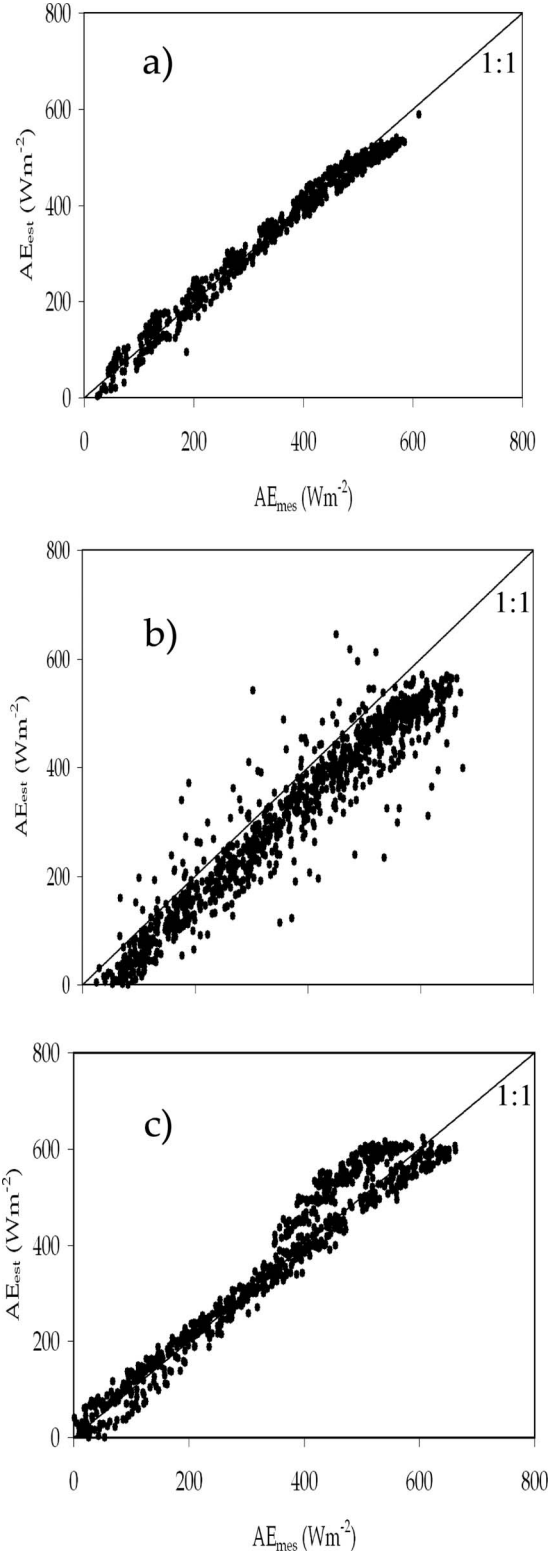

Figure 8. Comparison between estimated (*AE*$_{est}$) and measured (*AE*$_{mes}$) available energy over the three sites Agdal (a), R3 (b), and Sâada (c).

explained by the combination of several factors. Firstly, the use of the local estimated available energy at the scintillometer footprint scale can introduce an extra error. In practice, we need to aggregate the
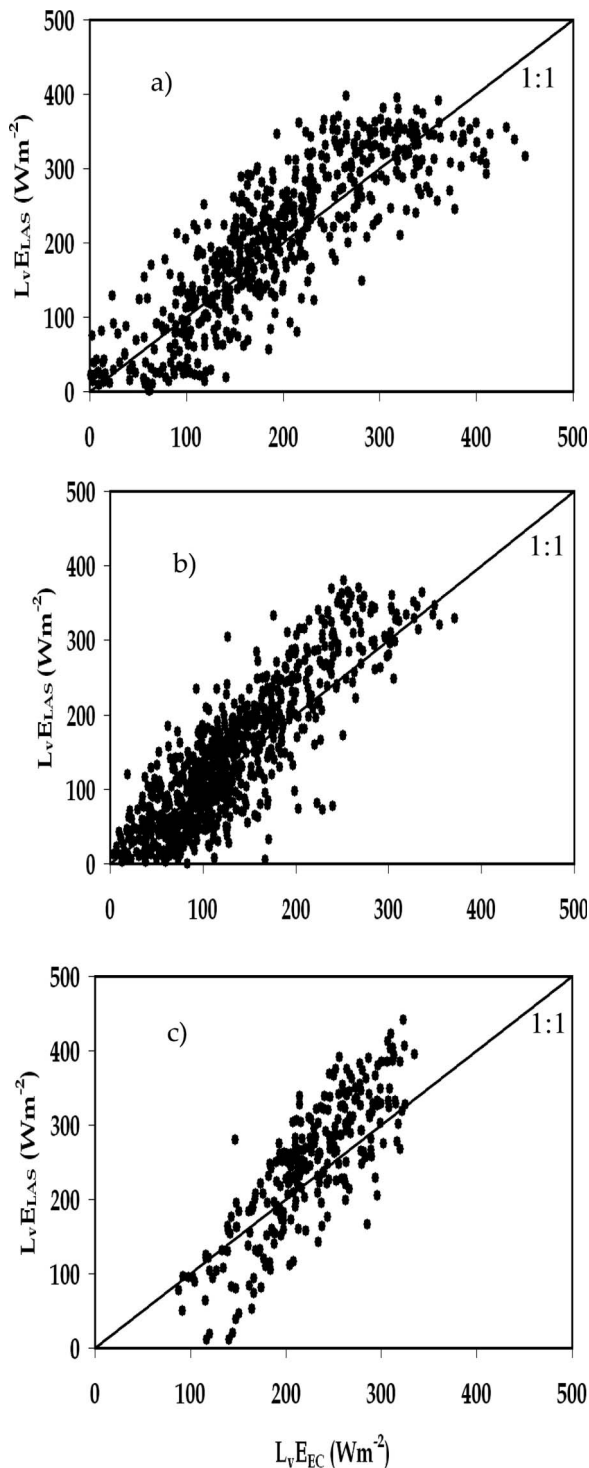
Figure 9. Comparison of L_vE_{EC} and L_vE_{LAS} (derived from the LAS using the estimated available energy) for Agdal (a), R3 (b) and Sâada (c) sites.

estimated AEest along the LAS path in order to fulfill the required condition of energy conservation. Secondly, the different characteristics between the source areas of LAS and EC (due to the irrigation method which created a large heterogeneity in soil moisture) greatly influences the correspondence between measured and simulated latent heat fluxes.

The third explanation can be related to the error associated with the closure of the measured energy balance, which can lead to errors in the simulated L_vE_{LAS}. Since the scintillometer-based L_vE_{LAS} is obtained as the residual term of the energy balance, any difference between measured and simulated available energy is directly translated into error in the simulated L_vE_{LAS}. Nevertheless, the results showed that, at least under the prevailing conditions at this study site, the combination of the LAS and the estimate of available energy leads to reasonably good estimates of area averaged latent heat flux over heterogeneous surfaces.

Conclusions

In this paper, a combination of scintillometer measurements and an estimate of available energy has been used to simulate the latent heat flux over the three dominant crops in the Tensift Al Haouz plain in Morocco. A comparison between the EC- and scintillometer-based estimates of the half-hourly sensitive heat fluxes during the dry conditions showed the potential of the large aperture scintill-ometer for estimating the spatial averaged sensible heat over both tall and sparse and short vegetation. During the irrigation events, a large part of the obtained discrepancy between H_{LAS} and H_{EC} can be attributed to the difference in the characteristics of the source areas of the LAS and EC system generated by the irrigation method. The comparison between the latent heat flux simulated by LAS (using the estimated available energy) and that measured by the EC system yields some discrepancies. However, considering the effect of irrigation, which created a large difference in the characteristics of the sources areas of LAS and EC, the lack of the energy balance closure of the EC measurements, and the uncertainty of the model used to estimate the available energy, the agreement between the simulated and measured latent heat fluxes is encouraging.

The above results have promising implications for practical applications. In fact one of the criteria for assessing irrigation efficiency is that the ratio between crop water requirement (ET_c) and actual ET should be as close to 1 as possible. Therefore, estimates of large-scale ET is of great importance for improving irrigation management, which will favourably impact the sustainability of water management in semi-arid regions.

References

Angstrom A. 1918. A study of the net radiation of the atmosphere. Smithsonian Inst Misc Coll 65: 159–161.

Asanuma J, Lemoto K. 2006. Measurements of regional sensible heat flux over Mongolian grassland using large aperture scintillometer. J Hydrol 333: 58–67.

Bastiaanssen WGM, Molden DJ, Makin IW. 2000. Remote sensing for irrigated agriculture: Eexamples from research and possible applications. Agric Water Mgmt 46: 137–155.

Brunt D. 1932. Notes on radiation in the atmosphere. Q J R Meteorol Soc 58: 389–418.

Brutsaert W. 1975. On a derivable formula for long-wave radiation from clear skies. Water Res Res 11: 742–744.

Brutsaert W. 1982. Evaporation into the atmosphere. Dordrecht: Reidel.

Centritto M, Loreto F, Massacci A, Pietrini F, Villani MC, Zacchini M. 2000. Improved growth and water use efficiency of cherry saplings under reduced light intensity. Ecol Res 15: 385–392.

Centritto M, Wahbi S, Serraj R, Chaves MM. 2005. Effects of partial rootzone drying (PRD) on adult olive tree (*Olea europaea*) in field conditions under arid climate. II. Photo-synthetic responses. Agric Ecosyst Envir 106: 303–311.

Chehbouni A, Kerr YH, Watts C, Hartogensis O, Goodrich DC, Scott R, et al. 1999. Estimation of area- average sensible heat flux using a large aperture scintillometer. Water Res Res 35: 2505–2512.

Chehbouni A, Watts C, Kerr YH, Dedieu G, Rodriguez JC, Santiago F, et al. 2000. Methods to aggregate turbulent fluxes over heterogeneous surfaces: Application to SALSA data set in Mexico. Agric For Meteorol 105: 133–144.

Chehbouni A, Escadafal R, Boulet G, Duchemin B, Simonneaux V, Dedieu G, et al. 2008a. The use of remotely sensed data for integrated hydrological modeling in arid and semi-arid regions: The SUDMED Program. Int J Rem Sensing, in press. ④

Chehbouni A, Ezzahar J, Watts C, Rodriguez JC, Garatuza-Payan J. 2008b. Estimating area-averaged surface fluxes over con-trasted agricultural patchwork in a semi-arid region. In: Hill J, Röder A, editors. Advances in remote sensing and geoinforma-tion processing for land degradation assessment. London: Taylor and Francis.

Chehbouni A, Hoedjes J, Rodriguez JC, Watts C, Garatuza-Payan J, Kerr YH. 2008c. Remote sensing based estimates of daytime area averaged surface fluxes over contrasted agricultural patchwork in a semi-arid region. Agric For Meteorol, http://dx.doi.org/10.1016/j.agrformet.2007.09.014, in press. ④

Clifford SF, Ochs GR, Lawrence RS. 1974. Saturation of optical scintillation by strong turbulence. J Opt Soc Am 71: 227–245.

De Bruin HAR, Kohsiek W, van den Hurk BJJM. 1993. A verification of some methods to determine the fluxes of momentum, sensible heat and water vapour using standard deviation and structure parameter of scalar meteorological quantities. Boundary Layer Meteorol 63: 231–257.

Duchemin B, Hadria R, Er-Raki S, Boulet G, Maisongrande P, Chehbouni A, et al. 2006. Monitoring wheat phenology and irrigation in Central Morocco: On the use of relationship between evapotranspiration, crops coefficients, leaf area index and remotely-sensed vegetation indices. Agric Water Mgmt 79: 1–27.

Er-Raki S, Chehbouni A, Guemouria N, Duchemin B, Ezzahar J, Hadria R. 2007. Combining FAO-56 model and ground-based remote sensing to estimate water consumptions of wheat crops in a semi-arid region. Agric Water Mgmt 87: 41–54.

Ezzahar J, Chehbouni A, Hoedjes JCB, Chehbouni A. 2007a. On the application of scintillometry over heterogeneous surfaces. J Hydrol 34: 493–501.

Ezzahar J, Chehbouni A, Hoedjes JCB, Er-Raki S, Chehbouni A, Bonnefond JM, et al. 2007b. The use of the Scintillation Technique for estimating and monitoring water consumption of olive orchards in a semi arid region. Agric Water Mgmt 89: 173–184.

Hill RJ, Ochs GR, Wilson JJ. 1992. Measuring surface-layer fluxes of heat and momentum using optical scintillation. Boundary Layer Meteorol 58: 391–408.

Hill RJ. 1997. Algorithms for obtaining atmospheric surface-layer fluxes from scintillation measurements. J Atmos Ocean Technol 14: 456–467.

Hoedjes JCB, Zuurbier RM, Watts CJ. 2002. Large aperture scintillometer used over a homogeneous irrigated area, partly affected by regional advection. Boundary Layer Meteorol 105: 99–117.

Hoedjes JCB, Chehbouni A, Ezzahar J, Escadafal R, De Bruin HAR. 2007. Comparison of large aperture scintillometer and eddy covariance measurements: Can thermal infrared data be used to capture footprint induced differences? J Hydrometeorol 8: 144–159.

Horst TW, Weil JC. 1994. How far is far enough? The fetch requirements for micrometeorological measurement of surface fluxes. J Atmos Ocean Technol 11: 1018–1025.

Horst TW. 1999. On frequency response corrections for eddy covariance flux measurements. Boundary Layer Meteorol 94: 517–520.

Humes KS, Kustas WP, Moran MS, Nichols WD, Weltz MA. 1994. Variability of emissivity and surface-temperature over a sparsely vegetated surface. Water Res Res 30: 1299–1310.

Idso SB. 1981. A set of equations for full spectrum and 8 to 14 mm and 10.5 to 12.5 mm thermal radiation from cloudless skies. Water Res Res 17: 295–304.

Kustas WP, Daughtry CST. 1989. Estimation of the soil heat flux/net radiation ratio from spectral data. Agric For Meteorol 49: 205–223.

Kustas WP, Goodrich DC. 1994. Special section – Monsoon 90 multidisciplinary experiment – Preface. Water Res Res 30: 1211–1225.

Kustas WP, Prueger JH, Hipps LE, Hatfield JL, Meek D. 1998. Inconsistencies in net radiation estimates from use of several models of instruments in a desert environment. Agric For Meteorol 90: 257–263.

Lagouarde JP, Bonnefond JM, Kerr YH, McAneney KJ, Irvine M. 2002. Integrated sensible heat flux measurements of a two-surface composite landscape using scintillometry. Boundary Layer Meteorol 105: 5–35.

Meijninger WML, Hartogensis OK, Kohsiek W, Hoedjes JCB, Zuurbier RM, De Bruin HAR. 2002a. Determination of area-averaged sensible heat fluxes with a large aperture scintill-ometer over a heterogeneous surface – Flevoland field experiment. Boundary Layer Meteorol 105: 37–62.

Meijninger WML, Green AE, Hartogensis OK, Kohsiek W, Hoedjes JCB, Zuurbier RM, et al. 2002b. Determination of area-averaged water vapour fluxes with a large aperture and radio wave scintillometers over a heterogeneous surface – Flevoland field experiment. Boundary Layer Meteorol 105: 63–83.

Monteith JL. 1973. Principles of environmental physics. London: Edward Arnold Press.

Monteith JL, Unsworth MH. 1990. Principles of environmental physics. London: Edward Arnold.

Moore CJ. 1986. Frequency response corrections for eddy correlation systems. Boundary Layer Meteorol 37: 17–35.

Norman JM, Kustas WP, Humes KS. 1995. A two-source approach for estimating soil and vegetation energy fluxes from observations of directional radiometric surface temperature. Agric For Meteorol 77: 263–293.

Ortega-farias S, Antonioletti R, Olioso A. 2000. Net radiation model evolution at an hourly time step for Mediterranean conditions. Agronomie 20: 157–164.

Panofsky HA, Dutton JA. 1984. Atmospheric turbulence: Models and methods for engineering applications. New York: John Wiley and Sons.

Schotanus P, Nieuwstadt F, De Bruin HAR. 1983. Temperature measurement with a sonic anemometer and its application to heat and moisture fluxes. Boundary Layer Meteorol 26: 81–93.

Scott RL, Eric A, Edwards EA, Shuttleworth WJ, Huxman TE, Watts C, et al. 2003. Interannual and seasonal variation in fluxes of water and carbon dioxide from a riparian woodland ecosystem. Agric For Meteorol 122: 65–84.

Stull RB. 1988. An introduction to boundary layer meteorology, atmospheric sciences. Dordrecht: Kluwer Academic Publishers.

Su Z, Schmugge T, Kustas WP, Massman WJ. 2001. An evaluation of two models for estimation of the roughness height for heat transfer between the land surface and the atmosphere. J Appl Meteorol 40: 1966–1951.

Tahi H, Wahbi S, Wakrim R, Aganchich B, Serraj R, Centritto M. 2007. Water relations, growth, photosynthesis and water use efficiency in tomato plant subjected to partial rootzone drying (PRD) and regulated deficit irrigation (RDI). Plant Biosyst 141: 265–274.

Testi L, Villalobos FJ, Orgaz F. 2004. Evapotranspiration of a young irrigated olive orchard in southern Spain. Agric For Meteorol 121: 1–18.

Twine TE, Kustas WP, Norman JM, Cook DR, Houser PR, Meyers TP, et al. 2000. Correcting eddy–covariance flux underestimates over a grassland. Agric For Meteorol 103: 279–300.

Van Dijk A, Kohsiek W, De Bruin HAR. 2003. Oxygen sensitivity of krypton and lymann-α hygrometers. J Atmos Ocean Technol 20: 143–151.

Villalobos FJ, Orgaz F, Testi L, Fereres E. 2000. Measurement and modeling of evapotranspiration of olive (*Olea europaea* L.) orchards. Eur J Agron 13: 155–163.

Webb EK, Pearman GI, Leuning R. 1980. Correction of flux measurements for density effects due to heat and water vapour transfer. Q J R Meteorol Soc 106: 85–100.

Wesely ML. 1976. The combined effect of temperature and humidity fluctuations on refractive index. J Appl Meteorol 15: 43–49.

Wilczak J, Oncley S, Stage SA. 2001. Sonic anemometer tilt correction algorithms. Boundary Layer Meteorol 99: 127–150.

Williams DG, Cable W, Hultine K, Hoedjes JCB, Yepez EA, Simonneaux V, et al. 2004. Evapotranspiration components determined by stable isotope, sap flow and eddy covariance techniques. Agric For Meteorol 125: 241–258.

Wilson K, Goldstein A, Falge E, Aubinet M, Baldocchi D, Berbigier P, et al. 2002. Energy balance closure at FLUXNET sites. Agric For Meteorol 113: 223–243.